AFRL-RV-PS-
TR-2011-0054

AFRL-RV-PS-
TR-2011-0054

THEORETICAL STUDIES OF LIGHT SCATTERING FROM SOLIDS, FILMS AND SURFACES

Godfrey Gumbs

Hunter College of the City University of New York
Department of Physics and Astronomy
695 Park Avenue
New York, NY 10065

18 May 2011

Final Report

AIR FORCE RESEARCH LABORATORY
Space Vehicles Directorate
3550 Aberdeen Ave SE
AIR FORCE MATERIEL COMMAND
KIRTLAND AIR FORCE BASE, NM 87117-5776

DTIC COPY

NOTICE AND SIGNATURE PAGE

AFRL-RV-PS-TR-2011-0054 HAS BEEN REVIEWED AND IS APPROVED FOR PUBLICATION IN ACCORDANCE WITH ASSIGNED DISTRIBUTION STATEMENT

//SIGNED//
DANHONG HUANG
Program Manager

//SIGNED//
PAUL D. LEVAN, Ph.D.
Technical Advisor, Space Based Advanced Sensing and Protection

//SIGNED//
B. SINGARAJU, Ph.D.
Deputy Chief, Spacecraft Technology Division
Space Vehicles Directorate

REPORT DOCUMENTATION PAGE

Form Approved
OMB No. 0704-0188

1. REPORT DATE *(DD-MM-YY)*	2. REPORT TYPE	3. DATES COVERED *(From - To)*
18-05-2011	Final Report	10-04-2008 – 24-02-2011

4. TITLE AND SUBTITLE
Theoretical Studies of Light Scattering from Solids, Films and Surfaces

5a. CONTRACT NUMBER
FA9453-07-C-0207

5b. GRANT NUMBER

5c. PROGRAM ELEMENT NUMBER
62601F

6. AUTHOR(S)
Godfrey Gumbs

5d. PROJECT NUMBER
4846

5e. TASK NUMBER

5f. WORK UNIT NUMBER
299286

7. PERFORMING ORGANIZATION NAME(S) AND ADDRESS(ES)
Hunter College of the City
University of New York
Department of Physics and Astronomy
695 Park Avenue
New York, NY 10065
New York, NY 10065

8. PERFORMING ORGANIZATION REPORT NUMBER

9. SPONSORING / MONITORING AGENCY NAME(S) AND ADDRESS(ES)
Air Force Research Laboratory
Space Vehicles Directorate
3550 Aberdeen Ave., SE
Kirtland AFB, NM 87117-5776

10. SPONSOR/MONITOR'S ACRONYM(S)
AFRL/RVSS

11. SPONSOR/MONITOR'S REPORT NUMBER(S)
AFRL-RV-PS-TR-2011-0054

12. DISTRIBUTION / AVAILABILITY STATEMENT
Approved for public release; distribution is unlimited. (377ABW 2011-0760, dated 24 May 2011)

13. SUPPLEMENTARY NOTES

14. ABSTRACT
We've investigated the conditions necessary to achieve strong plasmon instability at low temperature leading to emission in the terahertz regime for quantum wells. The surface response function was calculated for a bilayer two-dimensional electron gas (2DEG) system under a metal grating placed on the surface and which modulates the electron density. The 2DEG layers are coupled to surface plasmons arising from excitations of free carriers in the bulk region between the layers. A current is passed through one of multiple layers and is characterized by a drift velocity. We have also been investigating a system with relativistic like dispersion, e.g. graphene. The plasma excitations change considerably when the Fermi energy is at or close to the Dirac point. Several properties of graphene and graphene nanoribbons, e.g. the ballistic conductances optical conductivity, tunneling, effect of magnetic field on the plasmon excitations, and possible Bose-Einstein condensation in a double layer configuration were the subjects of our published works.

15. SUBJECT TERMS
optical signatures; scattering; near-field scattering; far-field scattering; plasmons; photoemission spectra

16. SECURITY CLASSIFICATION OF:			17. LIMITATION OF ABSTRACT	18. NUMBER OF PAGES	19a. NAME OF RESPONSIBLE PERSON
a. REPORT	b. ABSTRACT	c. THIS PAGE			Danhong Huang
Unclassified	Unclassified	Unclassified	Unlimited	32	19b. TELEPHONE NUMBER *(include area code)*

Standard Form 298 (Rev. 8-98)
Prescribed by ANSI Std. 239.18

(This page intentionally left blank)

TABLE OF CONTENTS

LIST OF FIGURES

LIST OF FIGURES CONTINUED

Figure **Page**

(This page intentionally left blank)

1. INTRODUCTION

Below, I give a brief summary of some of the related publications which were written during this contract with the AFRL. The work was conducted on both semiconductor heterostructures and graphene, whose energy band structure is shown schematically in Fig. 1. The calculations we report here for graphene and graphene nanoribbons took the hexagonal lattice structure into account. This is depicted in Fig. 2.

Some of our focus was on the conventional 2DEG with dispersion fully characterized by the electron effective mass and density in the conduction band. More recently, we turned our attention to the problem of response from the relativistic 2DEG. A good candidate to provide such an electron gas is graphene. Since graphene is a truly 2D system, it is informative to briefly compare it with the conventional 2DEG. Both of them provide two types of excitations: electron-hole pairs and collective modes such as plasmons. Electron-hole pairs are incoherent excitations of the Fermi sea and a direct consequence of the Pauli exclusion principle along with neglecting Coulomb interactions. Those exist whenever the polarization satisfies $\Im m\ \Pi^{2D} \neq 0$. On the other hand, the plasmons are related to the screening mechanism. If a test charge is placed in the 2DEG, the mobile electrons are set into motion in order to screen its electric field. As a result of the finite electron effective mass, they overshoot and the electron density starts to oscillate. Due to the absence of the mass of the Dirac electrons, one can assume that the plasmon oscillations in graphene should be qualitatively different from those of a conventional 2DEG.

In a system with relativistic-like dispersion $E = \pm v_F|k|$, such as graphene, these plasma excitations change considerably when the Fermi level is at or close to the Dirac point. In this case, the Fermi surface shrinks to a point and only inter-band transitions between the lower and upper part of the cone are allowed. Therefore, there are no electron-hole excitations at low energy ($\omega < v_F k$). Each excitation costs energy and the electron-hole continuum occupies the upper part of the energy ($\hbar\omega$) vs. momentum (k) diagram.

We also carried out a careful study of the electronic subband structure of InAs/GaSb based type II and broken-gap quantum well systems. Additionally, we reported on the band hybridization and spin-splitting in InAs/AlSb/GaSb type II and broken-gap quantum wells. Our obtained results will give us a clearer understanding of potential device applications and their potential for use as sensors.

This contract was a successful collaboration between AFRL and Hunter College/City University of New York (CUNY). In addition to the large number of published refereed publications and conference abstracts, invited and contributed talks at international conferences, Dr. Huang and I wrote a textbook on the techniques we employed in our research. This will be published by Wiley VCH in 2011. The cover of this book is appended (see Fig. A-1) in the Appendix) along with a flyer of a Workshop we are organizing in Spain in August, 2011 (see Fig. A-2 in the Appendix) as well as the front cover of a special issue on graphene (see Fig. A-3 in the Appendix).

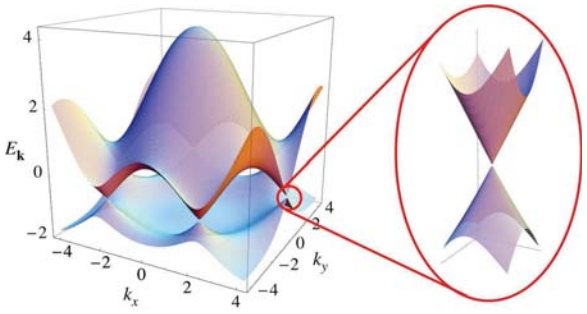

FIG. 1: Schematic of the energy band structure of graphene near the K-point.

In this report, we will first present the studies for the electron dynamics in different low-dimensional semiconductor systems. This part includes: the Bloch oscillation in quantum-dot superlattices that allows the optimal design of coherent terahertz emitter and detector for secured pilot communication and distant IED/explosive detection; the elastic/inelastic scattering of conduction electrons in quantum wires that allows the fabrication of high-speed electronics for on-chip signal processing; the spin entanglement of interacting electrons in a quantum dot driven by a surface acoustic wave that has potential applications in secured optical communication and encryption; the field-driven plasma instability in two-dimensional electron gas that can be used for tunable emission and detection, as well as coherent amplification of signal, in the terahertz and far-infrared frequency regimes; and the effect of spin-orbit interaction on thermoelectric power of electrons in quantum wires that can be employed for the design on-chip cooling of photodetectors. After this, we will present the studies for the electron dynamics in novel two-dimensional graphene materials. This part include: the induced energy gap in graphene quantum-dot array that has a very important

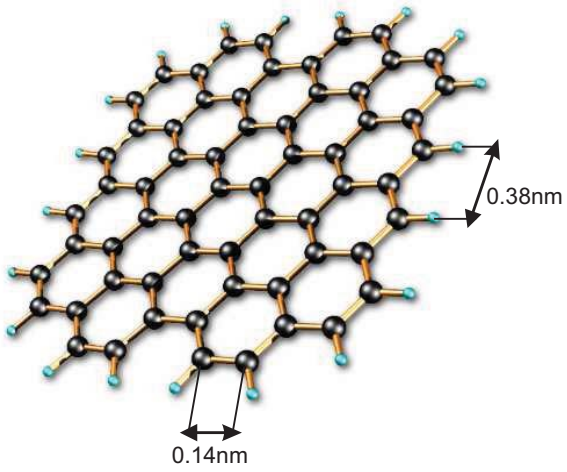

FIG. 2: Lattice structure of graphene.

application to tunable photodetection from terahertz up to visible frequency regimes; the unimpeded tunneling of carriers in graphene nanoribbons that will allow the design of tunable p-n nano-junctions for both optoelectronics and ultra-speed electronics used for photodetectors and on-chip processors; and the tunable band structure of graphene nanoribbons by electric and magnetic fields that can be employed for the use of frequency-tunable detection.

2. DISCUSSION OF RESULTS

2.1 Low-Dimensional Semiconductor Physics

The studies of electron dynamics in different low-dimensional semiconductor systems will be addressed in this part. For example, the exploration of Bloch oscillation in quantum-dot superlattices will allow the optimal design of coherent terahertz emitter and detector for secured pilot communication and distant IED/explosive detection. The investigation of elastic/inelastic scattering of conduction electrons in quantum wires will allow the fabrication of high-speed electronics for on-chip signal processing. The exploration of spin entanglement of interacting electrons in a quantum dot driven by a surface acoustic wave has potential applications in secured optical communication and encryption. The searching for field-driven plasma instability in two-dimensional electron gas can be used for tunable emission and detection, as well as coherent amplification of signal, in the terahertz and far-infrared frequency regimes. The study for the effect of spin-orbit interaction on thermoelectric power of electrons in quantum wires can be employed for the design on-chip cooling of photodetectors.

2.1.1 Quantum oscillations in the high frequency magnetoacoustic response of a quasi-two-dimensional metal

In this work, we presented the results of a theoretical analysis of magnetic quantum oscillations of the velocity and attenuation of high frequency ultrasound waves traveling in quasi-two-dimensional (Q2D) conductors. We chose a geometry where both the wavevector of the longitudinal sound wave and the external magnetic field are directed along the axis of symmetry of the Fermi surface. Assuming a moderately weak Fermi surface corrugation, we showed that the oscillating correction to the sound velocity may include a special term besides an ordinary contribution originating from quantum oscillations of the charge carrier density of states at the Fermi surface. This additional term is generated by a phase stability resonance occurring when the charge carrier velocity in the direction of the wave propagation equals the sound velocity. The two oscillating contributions to the sound velocity are shown to differ in phase and shape, and they may have the same order of magnitude. The appearance of the extra term may bring about significant changes in magnetic quantum oscillations of the velocity of sound in Q2D conductors, especially at low temperatures. This work is closely related to our research on the optical probing of quantum dot structures which we now describe.

2.1.2 Bloch oscillation, dynamical localization, and optical probing of electron gases in quantum-dot superlattices in high electric fields

Numerical results were presented for the time-dependent and steady-state currents as well as a long-time average current in a strong nonlinear DC and AC electric field for an electron gas in a one-dimensional (1D) quantum-dot superlattice. A microscopic model is employed for the scattering of electrons by phonons and static impurities by means of the Boltzmann equation method. The DC results are favorably compared with recent exact analytic results based on a relaxation-time model for electron-phonon scattering. Our results demonstrate the different roles played by elastic and inelastic scattering on the damped Bloch oscillations as well as the nonlinear steady-state current and their opposite roles on the damped dynamical localization. We also find a suppression of dynamical localization by strong Bloch oscillations and new features in the Esaki-Tsu peaks in the presence of an AC electric field when electron scattering is not neglected. On the basis of calculated non-equilibrium electron distribution from the Boltzmann equation, a self-consistent-field approach is employed to establish a general formalism for the optical response of current-driven electrons in both the linear and nonlinear regimes to a 1D quantum-dot superlattice. The DC-field dependencies of both the peak energy and peak strength in the absorption spectrum for a 1D quantum-dot superlattice were calculated, from which we find: (1) both the peak energy and its strength are significantly reduced with increasing DC electric field; and (2) the peak energy and peak strength are enhanced anomalously by raising the temperature for the nonlinear transport of electrons when a strong DC electric field is applied. We now describe some of the numerical techniques employed in our studies of nonlinear transport in quantum wires.

2.1.3 Coupled force-balance and scattering equations for nonlinear transport in quantum wires

The coupled force-balance and scattering equations were derived and applied to study nonlinear transport of electrons subjected to a strong dc electric field in an elastic-scattering-limited quantum wire. Numerical results have demonstrated both field-induced heating-up and cooling-down behaviors in the nonequilibrium part of the total electron-distribution function by varying the impurity density or the width of the quantum wire. The obtained asymmetric distribution function in momentum space invalidates the application of the energy-balance equation to our quantum-wire system in the center-of-mass frame. The experimentally observed suppression of mobility by a driving field for the center-of-mass motion in the quantum-wire system has been reproduced. In addition, the thermal enhancement of mobility in the elastic-scattering-limited system has been demonstrated, in accordance with a similar prediction made for graphene nanoribbons This thermal enhancement has been found to play a more and more significant role with higher lattice temperature and becomes stronger for a low-driving field.

We now turn our attention to describing the research we conducted on single and few electron transport through narrow channels in semiconductor heterostructures, using high-frequency electrostatic pumps.

2.1.4 Spin-split excitation gap and spin entanglement of a pair of interacting electrons in a quantum dot

We calculated the energy eigenvalues, the spin-split excitation gap (energy separation between the spin-triplet excited state and the spin-singlet ground state) and the concurrence for two interacting electrons captured in a quantum dot (QD) formed by a giga hertz electron pump which is modeled by harmonic confining potentials. We found from our calculations a peak in the QD size dependence of the energy level for the spin-singlet ground state, indicating the effect due to Coulomb blockade. In addition, we observed a local minimum in the QD size-dependence of the spin-split excitation gap for a relatively narrow quasi-one-dimensional (1D) channel formed from an etched wire, but a strong positive peak for the spin-split excitation gap in its QD size dependence with a relatively wide 1D channel. From the existence of a robust spin-split excitation gap against both thermal fluctuation due to finite (low) temperatures and the nonadiabatic effect due to fast barrier variations, we predicted a spin-entangled electron pair inside the dynamical QD with a weak coupling to external leads. An interference-type experiment which employs a gate-controlled electron pump and a beam splitter is proposed to verify this prediction. For the electron pump, a sinusoidal radio-frequency signal is applied to the entrance gate of a two gated system over a narrow channel etched in a GaAs/AlGaAs heterostructure, where the measured current within the channel shows plateaus at Nef with $N = 1, 2, \cdots$ being the number of captured electrons in a QD, and f the frequency of the sinusoidal signal. See Figs. 3, 4 and 5. In Fig, 3(a), we show two captured electrons from below the Fermi level in the channel; in Fig. 3(b), we depict that one of the two entangled electrons in a quantum dot is lifted up and over the exit barrier. The horizontal solid line represents the position of the Fermi level in the channel. The size of the quantum dot changes with time when an RF sinusoidal signal is applied to the left gate, thereby causing the confining potential region forming the quantum dot to be lowered below the Fermi level and then rise again. In Fig. 4, we chose $\ell_y/a_0 = 5$. In (a), the red solid curve is for the spin-singlet ground state, while the blue dash-dot-dotted curve is for the spin-triplet excited state. The horizontal dashed line, on the other hand, represents the energy of spin-triplet excited state for

two noninteracting electrons. Here, the zero-energy point for a single electron is set at $\hbar\Omega_y/2$. In Fig. 5(a), a QD is defined by gates V_1 (with an AC voltage $V^{\rm AC}$ supposed on V_1) and V_2. Two paths P_1 and P_2 are created to allow each of the two spin-entangled electrons from the dot to be separated. Gate $V_{\rm CS}$ is used to open and close path P_2 and gate $V_{\rm BS}$ is used as a beam splitter for the detection stage of the spin-entangled electrons. In Fig. 5(b) a two-dimensional gray scale deferential plot of pumped current through a QD. The individual plateaus are marked on the plot. The frequency of the RF signal was set to $f = 310.6\,$MHz and the power $-10\,$dBm. The dotted white box indicates the regime where two electrons are trapped in the dot. The plateau marked by A indicates where only one of the electrons is pumped through the system and the plateau marked by B is where both electrons are pumped.

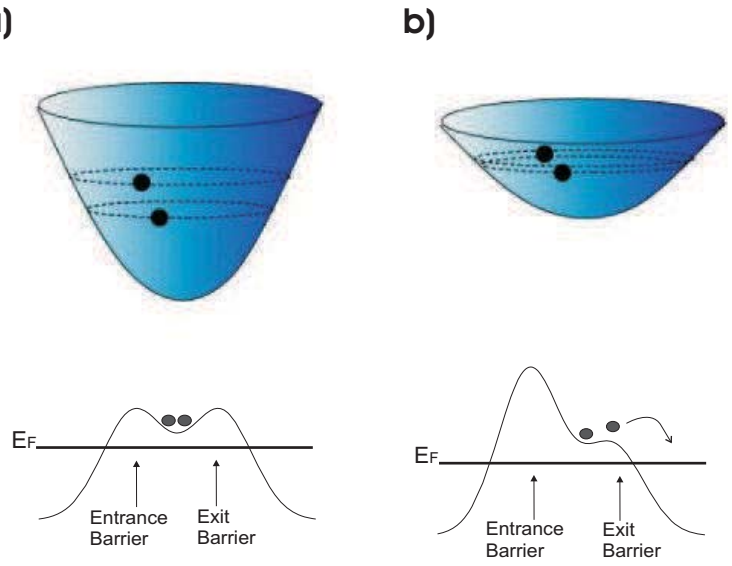

FIG. 3: Schematic illustration of the harmonic confining potential in 2D (lower) and 3D illustration (upper) with two captured electrons.

2.1.5 Enhanced optical probe of current-driven coupled quantum wells

In this project, we investigated the conditions necessary to achieve stronger Cherenkov-like instability of plasma waves leading to emission in the terahertz (THz) regime for semiconductor quantum wells (QWs). The surface response function is calculated for a bilayer two-dimensional electron gas (2DEG) system in the presence of a periodic spatial modulation of the equilibrium electron density. The 2DEG layers are coupled to surface plasmons arising from excitations of free carriers in the bulk region between the layers. A current is passed through one of multiple layers and is characterized by a drift velocity v_D for the driven electric charge. By means of a surface response function formalism, the plasmon dispersion equation is obtained as a function of frequency ω, the in-plane wave vector $\mathbf{q}_\parallel = (q_x, q_y)$ and reciprocal lattice vector nG where $n = 0, \pm1, \pm2, \cdots$ and $G = 2\pi/d$ with d denoting the period of the density modulation. The dispersion equation, which yields the resonant frequencies, is solved numerically in the complex ω-plane for real wave vector $\mathbf{q}_\parallel$. It is ascertained that the imaginary part of ω is enhanced with decreasing d, and with increasing the doping density of the free carriers in the bulk medium for fixed period of the spatial modulation. See Figs. 6, 7 and 8. In Fig. 6, the surface at $z = 0$ is covered by a grating (red lines) with period d and the width of the grating is assumed small compared to the period d. The doped barriers (AlGaAs) are the unshaded areas and quantum wells (GaAs, blue areas) in the z direction are indicated as the 2DEG layers. The system is embedded in a dielectric medium. In Fig. 7, the frequencies are expressed in units of ω_F and are plotted as functions of the in-plane wave vector $q_\parallel$ in units of k_F. The real solutions, shown in black, have several branches. The imaginary solutions are shown in red. No modulating potential was applied in these calculations. Only those plasmon frequencies with finite imaginary parts are presented. The parameters used in the calculations are given in the text with $\omega_p = 0.92\omega_F$.

2.1.6 Collective properties of excitons in the presence of a two-dimensional electron gas

In an effort to further understand the optical properties of semiconductor heterostructures, we studied the collective properties of two-dimensional (2D) excitons immersed within a quantum well which contains 2D excitons and a

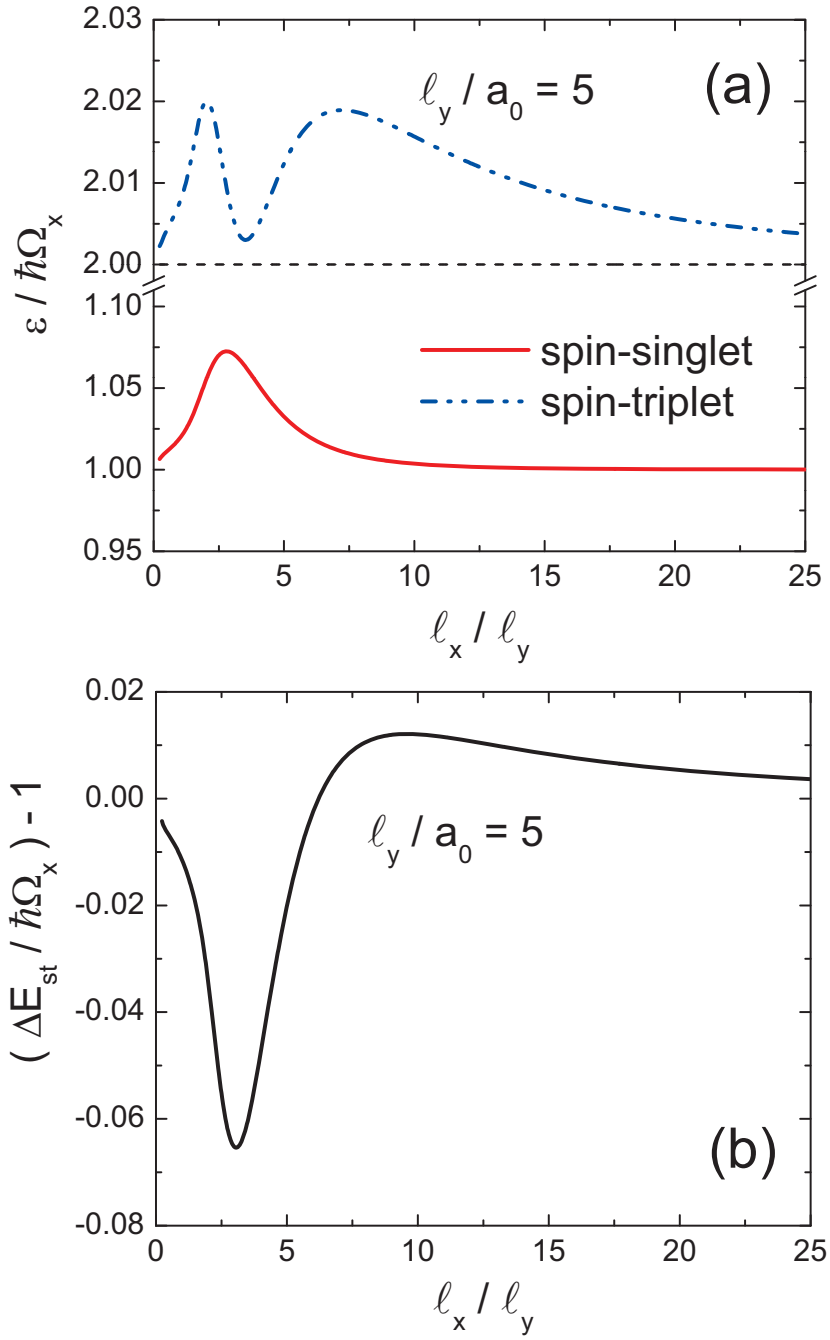

FIG. 4: (a) Two-interacting-electron energy eigenvalues $\varepsilon/\hbar\Omega_x$ [in (a)] and the deduced Coulomb effect on the spin-split excitation gap $(\Delta E_{\rm st} - \hbar\Omega_x)/\hbar\Omega_x$ [in (b)] as functions of the QD size ℓ_x/ℓ_y.

two-dimensional electron gas (2DEG). We have also analyzed the excitations for a system of 2D dipole excitons with spatially separated electrons and holes in a pair of quantum wells (CQWs) when one of the wells contains a 2DEG. Calculations of the superfluid density and the Kosterlitz-Thouless (K-T) phase transition temperature for the 2DEG-exciton system in a quantum well have shown that the K-T transition temperature increases with increasing exciton density and that it might be possible to have fast long range transport of excitons. The superfluid density and the K-T transition temperature for dipole excitons in CQWs in the presence of a 2DEG in one of the wells increases with increasing inter-well separation.

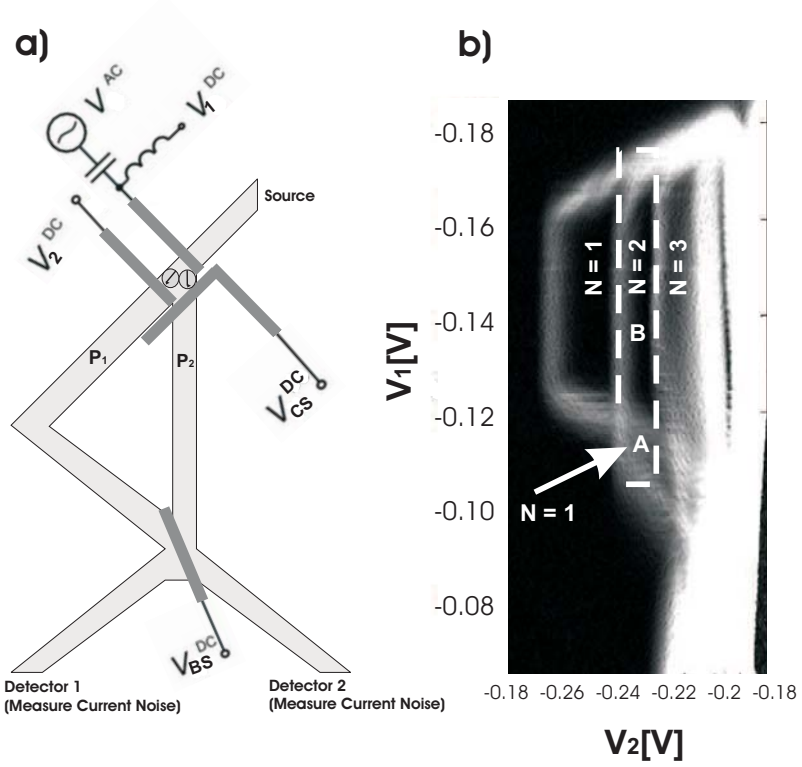

FIG. 5: (a) A schematic of a device that could be used to produce and measure spin-entangled electrons. (b) A two-dimensional gray scale deferential plot of pumped current through a QD ···

Figure 1

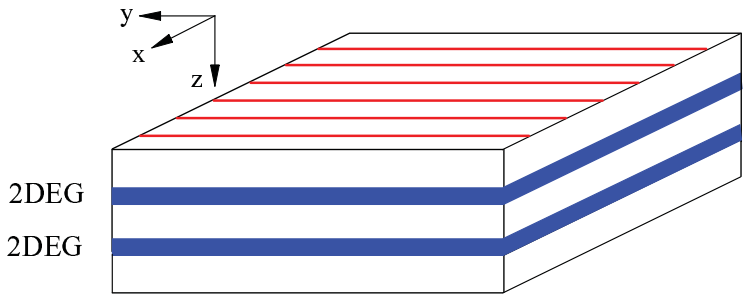

FIG. 6: Schematic illustration of a bilayer with an applied electrostatic modulation periodic in the x direction.

2.1.7 Comparison of inelastic and quasielastic scattering effects on nonlinear electron transport in quantum wires

When impurity and phonon scattering coexist, the Boltzmann equation has been solved exactly for nonlinear electron transport in a quantum wire. Based on the calculated non-equilibrium distribution of electrons in momentum space, the scattering effects on both the linear and nonlinear mobilities of electrons as functions of temperature and dc field were demonstrated. The linear mobility of electrons is switched from a linearly increasing of temperature to a parabolic-like temperature dependence as the quantum wire is tuned from an impurity-dominated system to a phonon-dominated one [see T. Fang, *et al.*, Phys. Rev. B **78**, 205403 (2008)]. In addition, a maximum has been obtained in the dc-field dependence of nonlinear mobility of electrons. The low-field mobility is dominated by impurity scattering, whereas the high-field mobility is limited by the phonon scattering [see M. Hauser, *et al.*, Semicond. Sci. Technol.

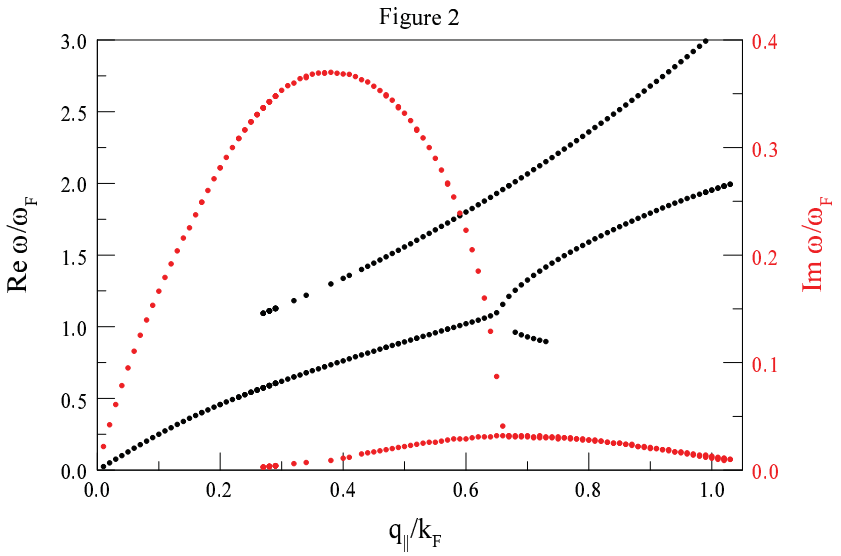

FIG. 7: Plots of the real (left scale) and imaginary (right scale) parts of the plasmon frequency for a bilayer 2DEG system with spacing $a = 100$ Å between the layers.

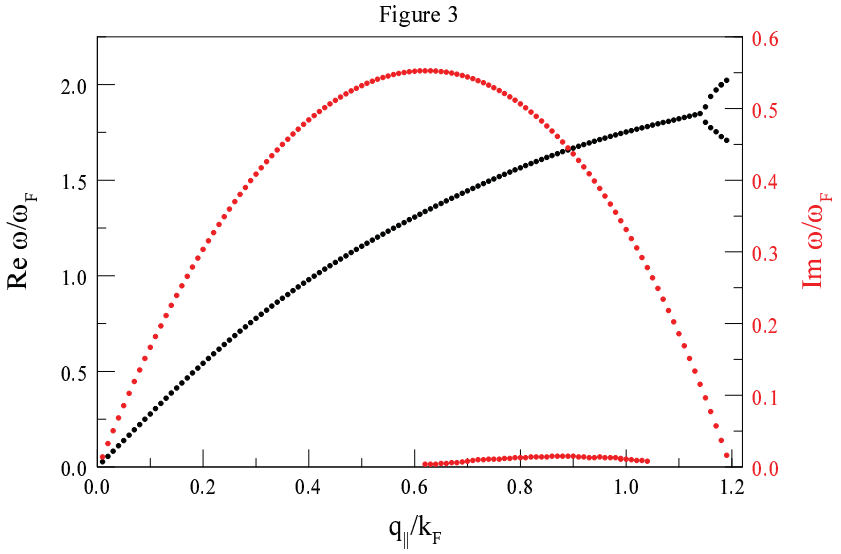

FIG. 8: The same as Fig. 7, except that the frequency $\omega_p = 1.84\omega_F$.

9, 951 (1994)]. Once a quantum wire is dominated by the elastic scattering, the peak of the distribution function becomes sharpened and both tails of the equilibrium electron distribution centered at the Fermi edges are raised by the dc field after a redistribution electrons in the momentum space is fulfilled in a symmetric way. If a quantum wire is dominated by the inelastic scattering, on the other hand, the peak of the distribution function is unchanged while both shoulders centered at the Fermi edges shift leftward correspondingly with increasing dc field through an asymmetric redistribution of the electrons in momentum space [see C. Wirner, *et al.*, Phys. Rev. Lett. **70**, 2609 (1993)].

2.1.8 Band hybridization and spin-splitting in InAs/AlSb/GaSb type II and broken-gap quantum wells

We conducted a detailed theoretical study on the features of band hybridization and zero-field spin splitting in InAs/AlSb/GaSb quantum wells (QWs) for possible use as semiconductor sensors. An eight-band $\mathbf{k} \cdot \mathbf{p}$ approach is developed to calculate the electronic subband structure in such structures. In the absence of the AlSb layer,

the hybridized energy gaps can be observed at the anti-crossing points between the ground electron subband and heavy-hole subband in respectively the InAs and GaSb layers. In such a case, the position and magnitude of the gaps are spin-dependent. When a thin AlSb layer is placed between the InAs and GaSb layers, we find that the ground electron subband in the InAs layer is now hybridized only with the ground light-hole subband which is also hybridized with the ground heavy-hole subband in the GaSb layer. The hybridized energy gaps and spin splitting in the InAs/AlSb/GaSb QWs are reduced significantly. These results can be used to understand why relatively high mobilities for electrons and holes can be achieved in InAs/AlSb/GaSb type II and broken gap QWs. The present study is relevant to the applications of InAs/GaSb based QW structures as new generation of high-density and high-mobility electronic devices. (See Figs 9, and 10.)

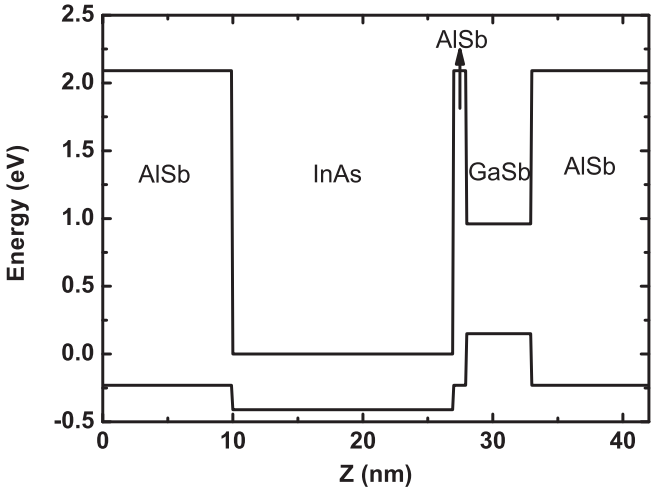

FIG. 9: Band alignment for an AlSb/InAs/AlSb/GaSb/AlSb type II and broken-gap quantum well.

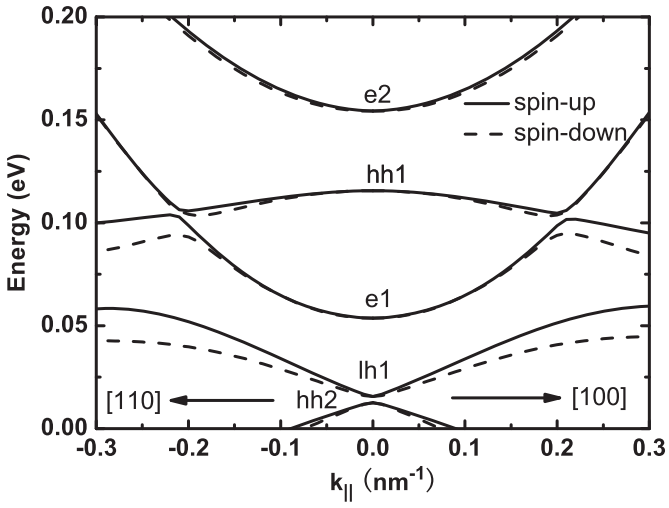

FIG. 10: The energy spectrum, $E_n(\mathbf{k}_\parallel)$, for electrons and holes in an AlSb/InAs/GaSb/AlSb quantum well as a function of the wavevector $k_\parallel$ at the fixed InAs/GaSb layer widths 17/5 nm. The solid and dashed curves are for spin-up and spin-down states.

2.1.9 Signatures of carrier multiplication in polariton fluorescence spectra

An innovative concept is the integration of solar cell with a photodetector through growth process for self-power supply on the pixel level. We would like to develop a hybrid quantum heterojunction-based solar cell system, which transforms solar energy as input to phase-coherent electric waves as output to minimize heat dissipation. Each hybrid quantum unit is a regular network of QDs. Each node is a QD with a surrounding subnetwork of quantum wells connected by quantum wires in a nearest-neighbor configuration. Energy and other quantities are realized in dynamic, controlled electron-hole configurations.

In our initial work, we investigated carrier multiplication (CM). The fundamental science is the creation of cavity exciton polariton in the strong coupling regime, carrier multiplication mechanism, driven plasma instability, Forster mechanism for inter-dot exciton energy exchange, as we now describe. Using the micro-cavity coupled to q-deformed bosons, we investigated the signatures of carrier multiplication in the single and two photon emitted frequency resolved florescence. Those are compared to the spectra provided by the conventional multi photon induced florescence. The two processes are distinguished by the statistics of the initial polariton distribution. We investigated all possible ranges of the exciton confinement above the saturation limit. For all of them the exciton emission spectra turned out to be CM insensitive, while the polaritons emission demonstrates strong spectral signatures of the CM.We concluded that in extremely weak confinement regime the increase in quantum yield leads to consecutive appearance of Rabi multiplets. The correlation spectra reveal one more multiplet as compared to the single photon emission. When the confinement increases the Rabi multiplets start to overlap and their classification requires transient measurements of the spectral snapshots. Those are based on the discrete Auger lifetimes of the multi-excitons. When the confinement is strong enough so that the bosonic picture of the excitons is strongly q-deformed the CM mechanism enhances the Mollow triplet commensurate with the Rabi doublet for the single polariton. (See Figs. 11)

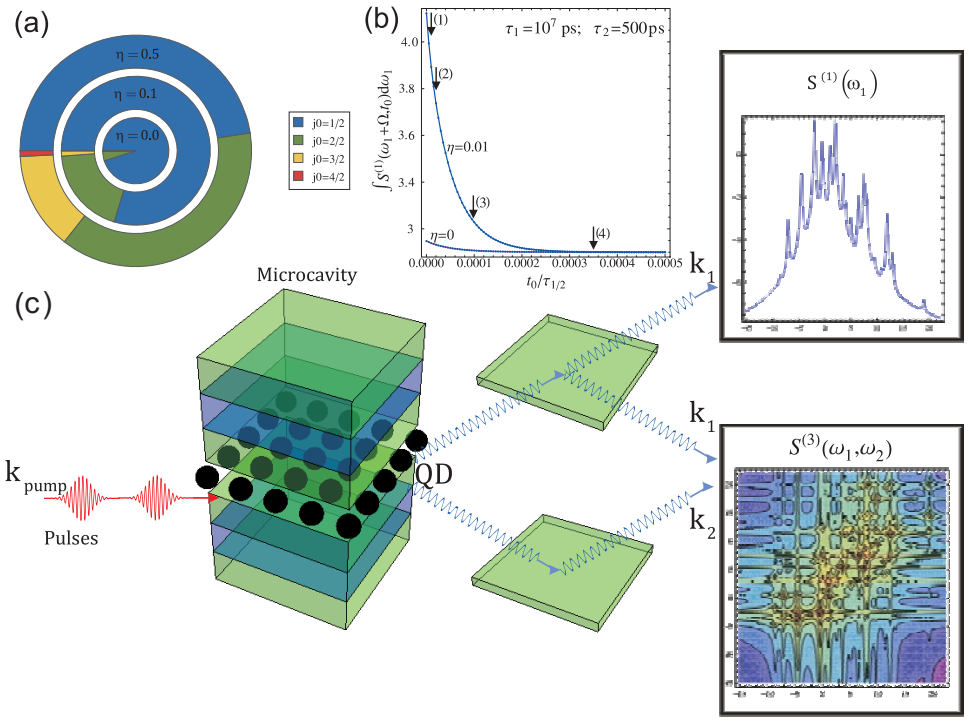

FIG. 11: Schematics of the multi-photon presence from the polariton states populated by CM.

2.1.10 IR modes in 2DEHGS magneto-infrared modes in InAs-AlSb-GaSb coupled quantum wells

The properties of hetrostructures under large magnetic field conditions would help in determining their suitability for device applications. So, in collaboration with an experimental group at the high magnetic field facility in Tallahassee, we studied a series of InAs/GaSb coupled quantum wells using magneto-infrared spectroscopy for high magnetic fields up to 33T within temperatures ranging from 4K to 45K in both Faraday and tilted field geometries. This type of coupled quantum wells consists of an electron layer in the InAs quantum well and a hole layer in the GaSb quantum

well, forming the so-called two dimensional electron-hole bilayer system. Unlike the samples studied in the past, the hybridization of the electron and hole subbands in our samples is largely reduced by having narrower wells and an AlSb barrier layer interposed between the InAs and the GaSb quantum wells, rendering them weakly hybridized. Previous studies have revealed multiple absorption modes near the electron cyclotron resonance of the InAs layer in moderately and strongly hybridized samples, while only a single absorption mode was observed in the weakly hybridized samples. We have observed a pair of absorption modes occurring only at magnetic fields higher than 14T that exhibited several interesting phenomena. Amongst this interesting phenomena we found two unique types of behavior that distinguishes this work from the ones reported in the literature. This pair of modes is very robust against rising thermal excitations and increasing magnetic fields aligned parallel to the heterostructures. While the previous results were aptly explained by the antilevel crossing gap due to the hybridization of the electron and hole wavefunctions, i.e. conduction-valence Landau level mixing, the unique features reported in this paper cannot be explained with the same concept. The unusual properties found in this study and their connection to the known models for InAs/GaSb heterostructures will be discussed; in addition, several alternative ideas will be proposed in this paper and it appears that a spontaneous phase separation can account for most of the observed features. See Fig. 12 for the measured cyclotron resonance at low magnetic fields and the anomalous splitting near filling factor $\nu = \frac{1}{2}$.

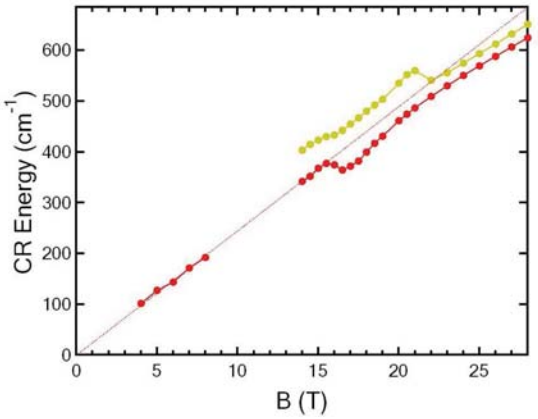

FIG. 12: The energies of the absorption modes as a function of magnetic field are displayed. The energy separation is about 60 cm^{-1} in zone (1), 80 cm^{-1} in zone (2) and 25 cm^{-1} in zone (3).

2.1.11 Energy bands, conductance and thermoelectric power for ballistic electrons in a nanowire with spin-orbit interaction

We calculated the effects of spin-orbit interaction (SOI) on the energy bands, ballistic conductance (G) and the electron-diffusion thermoelectric power ($S_{\rm d}$) of a nanowire by varying the temperature, electron density and width of the wire. The potential barriers at the edges of the wire are assumed to be very high. A consequence of the boundary conditions used in this model is determined by the energy band structure, resulting in wider plateaus when the electron density is increased due to larger energy-level separation as the higher subbands are occupied by electrons. The nonlinear dependence of the transverse confinement on position with respect to the well center excludes the "pole-like feature" in G which is obtained when a harmonic potential is employed for confinement. At low temperature, $S_{\rm d}$ increases linearly with T but deviates from the linear behavior for large values of T. (See Figs. 13, 14(a) and 14(b).)

2.2 Physics of Graphene and Nanotubes

The studies of electron dynamics in novel two-dimensional graphene materials will be addressed in this part. For example, the exploration of induced energy gap in graphene quantum-dot array has a very important application to tunable photodetection from terahertz up to visible frequency regimes. The investigation of unimpeded tunneling of carriers in graphene nanoribbons will allow the design of tunable p-n nano-junctions for both optoelectronics and ultra-speed electronics used for photodetectors and on-chip processors. The study of tunable band structure of graphene nanoribbons by electric and magnetic fields can be employed for the use of frequency-tunable detection.

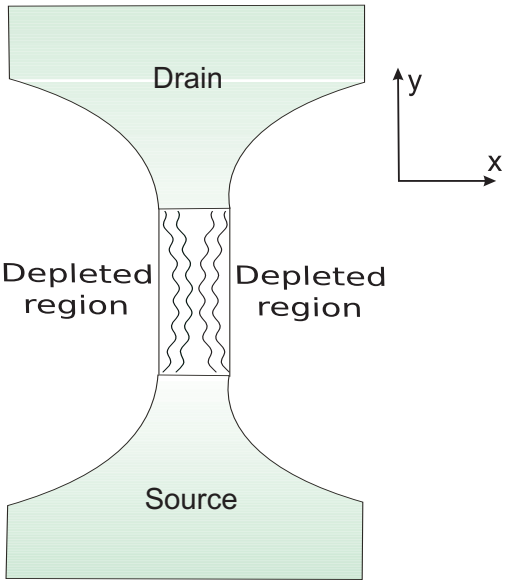

FIG. 13: Schematic illustration of the nanowire of 2DEG between a source and drain.

2.2.1 Quasiparticles for a quantum dot array in graphene and the associated magnetoplasmons

We calculated the low-frequency magnetoplasmon excitation spectrum for a square array of quantum dots on a two-dimensional (2D) graphene layer. The confining potential is linear in the distance from the center of the quantum dot. The electron eigenstates in a magnetic field and confining potential are mapped onto a 2D plane of electron-hole pairs in an effective magnetic field without any confinement. The tight-binding model for the array of quantum dots leads to a wavefunction with inter-dot mixing of the quantum numbers associated with an isolated quantum dot. For chosen confinement, magnetic field, wave vector and frequency, we plot the dispersion equation as a function of the period d of the lattice. We obtain those values of d which yield collective plasma excitations. For the allowed transitions between the valence and conduction bands in our calculations, we obtain plasmons when $d \lesssim 100\mathring{A}$. Not only did we start investigating the optical properties of graphene, but also its transport properties, as we now describe.

2.2.2 Unimpeded tunneling in graphene nanoribbons

We have analyzed the Klein paradox in zigzag (ZNR) and anti-zigzag (AZNR) graphene nanoribbons for transmission through a potential barrier. Due to the fact that ZNR (the number of lattice sites across the nanoribbon = N is even) and AZNR (N is odd) configurations are indistinguishable when treated by the Dirac equation, we supplemented the model with a pseudo-parity operator whose eigenvalues correctly depend on the sublattice wavefunctions for the number of carbon atoms across the ribbon, in agreement with the tight-binding model. We have shown that the Klein tunneling in zigzag nanoribbons is related to conservation of the pseudo-parity rather than pseudo-spin in infinite graphene. The perfect transmission in the case of head-on incidence is replaced by perfect transmission at the center of the ribbon and the chirality is interpreted as the projection of the pseudo-parity on momentum at different corners of the Brillouin zone. See Fig. 15.

2.2.3 Tunable band structure effects on ballistic transport in graphene nanoribbons

Another aspect of the electron transport was undertaken for graphene nanoribbons (GNR) in mutually perpendicular electric and magnetic fields showing dramatic changes in their band structure and electron transport properties. A strong electric field across the ribbon induces multiple chiral Dirac points, closing the semiconducting gap in armchair GNR's. A perpendicular magnetic field induces partially formed Landau levels as well as dispersive surface-bound states. Each of the applied fields on its own preserves the even symmetry $E_k = E_{-k}$ of the subband dispersion. When applied together, they reverse the dispersion parity to be odd and gives $E_{\mathrm{e},k} = -E_{\mathrm{h},-k}$ and mix the electron and hole subbands within the energy range corresponding to the change in potential across the ribbon. This leads to oscillations of the ballistic conductance within this energy range. In Fig. 16, panels (a) represent the dispersion curves for the electrons (green curves) in the conduction band and holes (blue curves) in the valence band. The lowest conduction

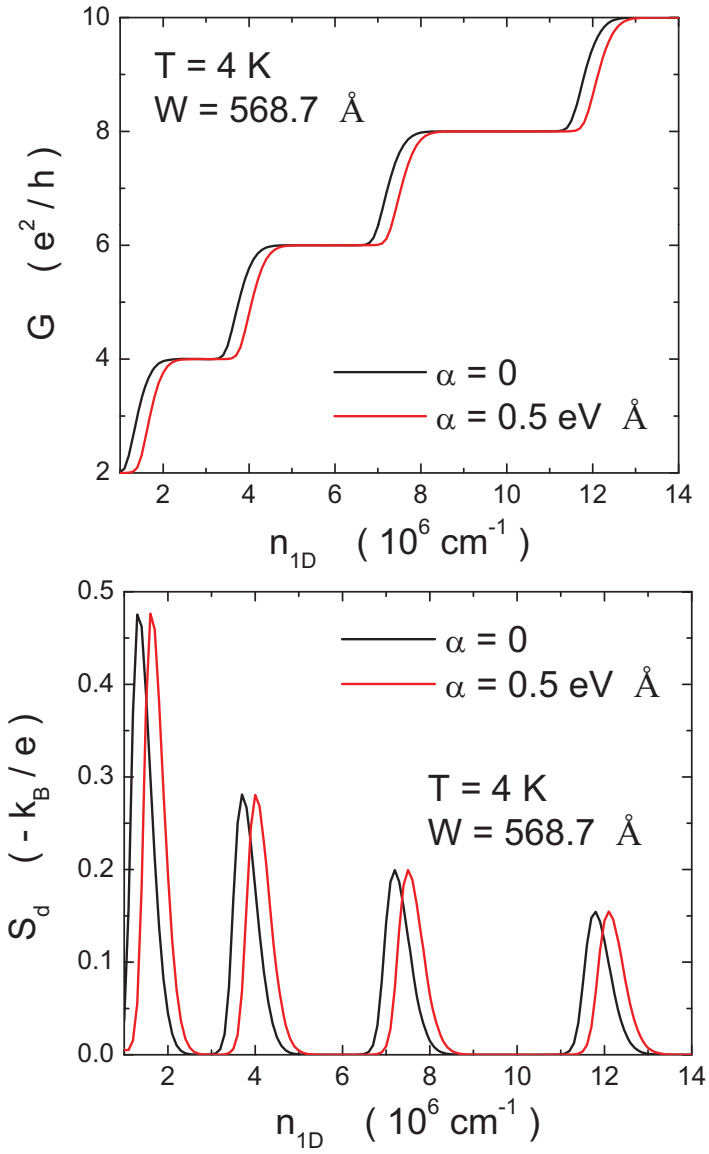

FIG. 14: Comparison of the conductance G (upper panel) to the electron-diffusion thermoelectric power $S_{\rm d}$ (lower panel), as a function of the electron density $n_{\rm 1D}$ with a wire width $\mathcal{W} = 568.7\,$Å and a temperature $T = 4\,$K for $\alpha = 0$ (black curves) and $\alpha = 0.5\,$eV·Å (red curves), respectively.

and highest valence subbands are given by the thick curves. Panels (b) shows local density of states. Panels (c) give the corresponding ballistic conductance in units of $2e^2/h$. Panels (1) correspond to absence of the em. field. Panels (2) correspond to the sole magnetic field of the flux through a single hexagon placket $\phi/\phi_0 = 1/150$. Panel (3) show the effect of the sole electric field of the strength $U_0/t_0 = 1/2$. Panels (4) demonstrate the combined effects due to an electric and magnetic field with the same strength as that employed in panels (2)-(3).

2.2.4 Spin-dependent scattering by a potential barrier on a nanotube

The electron spin effects on the surface of a nanotube have been considered through the spin-orbit interaction (SOI), arising from the electron confinement on the surface of the nanotube. This is of the same nature as the Rashba-Bychkov SOI at a semiconductor heterojunction. Using a continuum model, we obtained analytic expressions for the spin-split energy bands for electrons on the surface of nanotubes in the presence of SOI. We calculated analytically the scattering amplitudes from a potential barrier located around the axis of the nanotube into spin-dependent states. We investigated the dependence of tunneling and reflection on the height of the potential barrier, the angular and

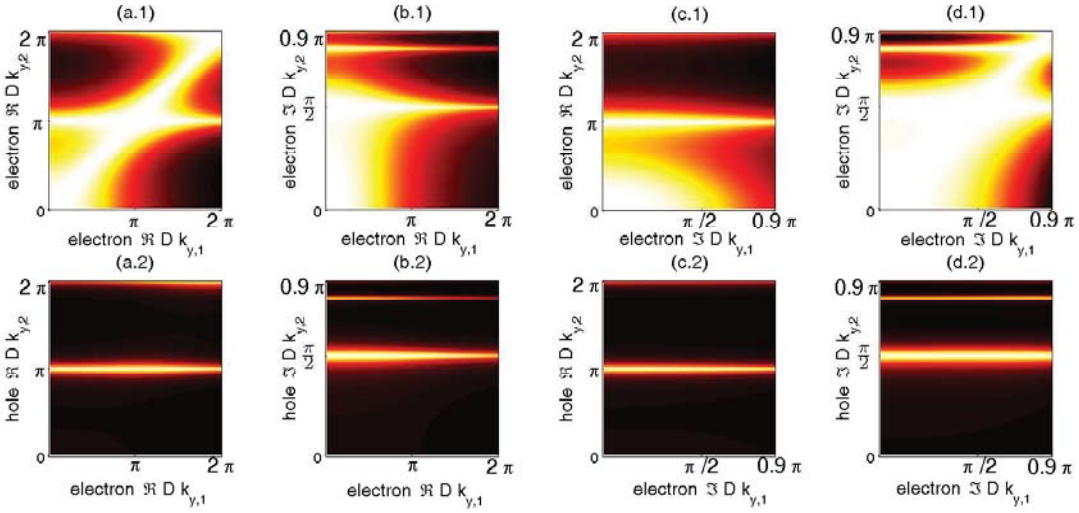

FIG. 15: The transmission $|t(k_{y,1}, k_{y,2})|^2$ for 9-AZNR non-chiral π electron. Panels (a.1)-(d.1) correspond to over the barrier transmission $E > V_0$.

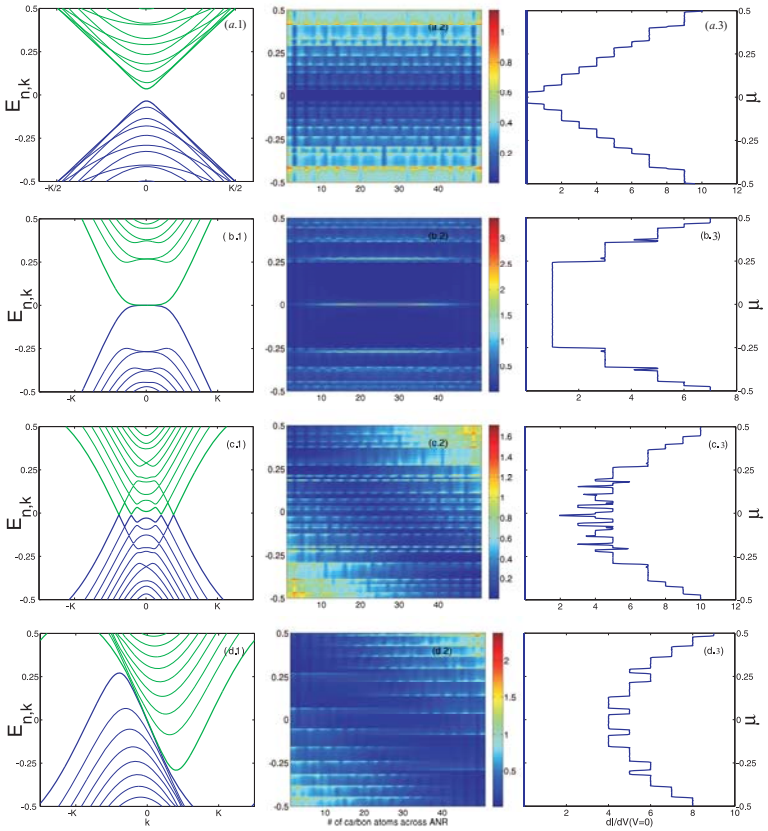

FIG. 16: Energy bands, local density of states and ballistic conductance of armchair nanoribbons in the presence of an in-plane electric field and/or perpendicular magnetic field.

linear momentum of the incoming particle, and its spin orientation. We demonstrated that perfect transmission may be achieved for certain barrier heights. (See Figs. 17, 18(a) and 18(b).)

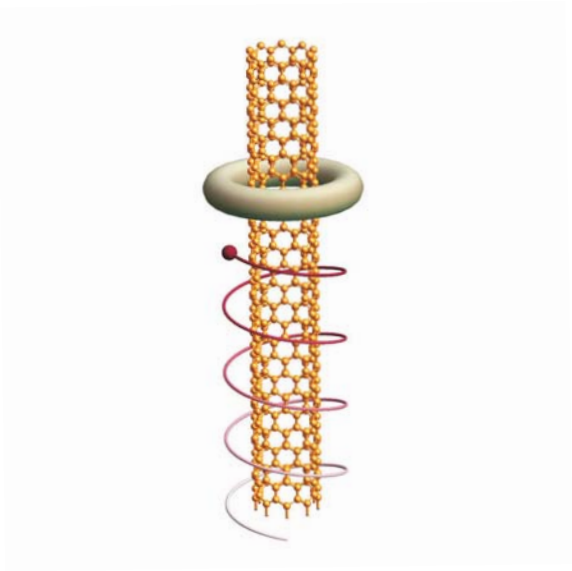

FIG. 17: Schematic illustration of the nanotube in the presence of a particle having linear momentum parallel to the axis of the nanotube as well as angular momentum around its axis. The incoming particle impinges on a barrier of uniform thickness .

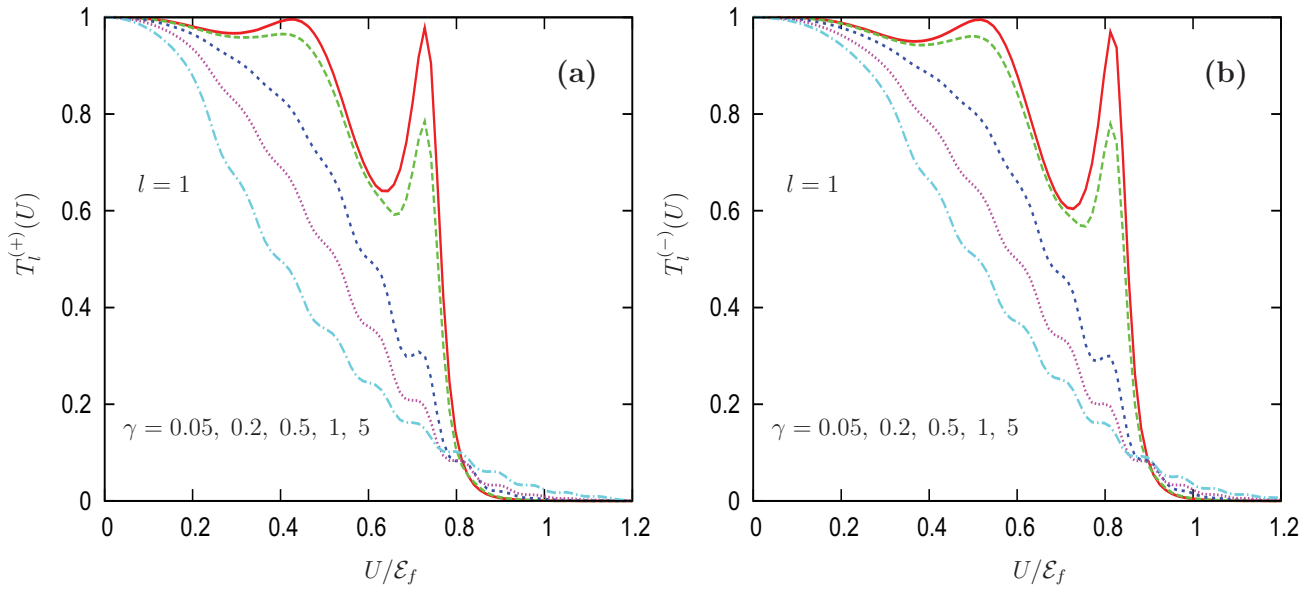

FIG. 18: Transmission Probabilities in the presence of impurities (defects) included phenomenologically via Eq. (27) of Ref. [8] listed above with the parameter γ related to temperature for (a) the "+" states and (b) the "$-$" for SOI $\mathcal{E}_\alpha = 0.08\mathcal{E}_f$.

3. CONCLUSIONS

In conclusion, we carefully conducted basic research into problems that were computationally intensive and required a team of researchers at the AFRL and CUNY to bring them to a stage that would be difficult to undertake by a single Principal Investigator (PI). Our focus was on the photonics and electron transport in graphene and semiconducting heterostructures. Specifically, we were engaged in studying (a) plasma instability in semiconductor heterostructures, (b) carrier multiplication in quantum dots and applications to solar cells, (c) single and few electron transport in semiconductor heterostructures, (d) nonlinear transport in systems with reduced dimensionality and (e) electron transport on carbon nanotubes. The budget was mainly used to support a post doctoral fellow, a graduate student and part-time undergraduates. Team coordination discussions were held at least once each week between CUNY and AFRL to brief each other on the progress made on our research and to discuss new directions. Wherever necessary,

there was a sharing of algorithms.

The electron dynamics in different low-dimensional semiconductor systems has been explored, which has a variety of defense-related applications. For example, the Bloch oscillation in quantum-dot superlattices facilitates the optimal design of coherent terahertz emitter and detector for secured pilot communication as well as the distant IED/explosive detection. The spin entanglement of interacting electrons in a quantum dot driven by a surface acoustic wave can be used for secured optical communication and encryption. In addition, the electron dynamics in two-dimensional graphene materials has also been explored, which has many novel applications. For example, the unimpeded tunneling of carriers in graphene nanoribbons will allow the design of tunable p-n nano-junctions for both optoelectronics and ultra-speed electronics used for photodetectors and on-chip processors. The tunable band structure of graphene nanoribbons by electric and magnetic fields can be employed for the use of frequency-tunable detection.

APPENDIX

A. Refereed Journal Publications

1. **Godfrey Gumbs** and D. H. Huang: *Electronically Modulated 2D Plasmons Coupled to Surface Plasmon Modes*, Physical Review B **75**, 115314 (1-9) (2007).

   $\longrightarrow$ {Selected for the March 26, 2007 issue of Virtual Journal of Nanoscale Science & Technology.}

2. **Godfrey Gumbs**, Yonatan Abranyos, and T. McNeish: *Plasma Excitations for Cylindrical Nanotubes with Spin Splitting*, Journal of Physics: Condensed Matter **19**, 106213-106222 (2007).

3. Yonatan Abranyos and **Godfrey Gumbs**: *The Enhancement of the Exchange Coupling by the Spin Orbit Interaction on Nanotubes*, Physical Review B **75**, 085404 (1-7) (2007).

   $\longrightarrow$ {Selected for the February 2007 issue of Virtual Journal of Quantum Information.}

4. W. Xu, P. A. Folkes, **Godfrey Gumbs**, Z. Zeng, and C. Zhang: *Electronic subband structure of InAs/GaSb based type II and broken- gap quantum well systems*, Physica E **40**, 1536-1539 (2007).

5. **Godfrey Gumbs** and Paula Fekete: *Frequency-Dependent Magnetotransport in a Modulated 2DES*, Advanced Studies in Theoretical Physics **1**, 467-487 (2007).

6. **Godfrey Gumbs** and E. Kogan: *Effect of Electron-electron Interaction and Plasmon Excitation on the Density-of-states for a Two-Dimensional Electron Liquid*, Physica Status Solidi B **244** 3695-3702 (2007).

7. W. Xu, P. A. Folkes, and **Godfrey Gumbs**: *Self-consistent electronic subband structure of undoped InAs/GaSb-based type II and broken-gap quantum well systems*, Journal of Applied Physics **102**, 033703 (1-7) (2007).

8. **Godfrey Gumbs**, A. Balassis: *Formula for the Absorption Coefficient for Multi-Wall Nanotubes*, Physics Letters A **372**, 3517-3524 (2008).

9. D. H. Huang, Paul M. Alsing, D. A. Cardimona, and **Godfrey Gumbs**: *Effects of Electronic Quantum Interference, Photonic-Crystal Cavity, Longitudinal Field and Surface-Plasmon-Polariton for Optical Amplification*, IEEE Trans. on Nanotechnology **7**, 151-164 (2008).

10. Natalya Zimbovskaya and **Godfrey Gumbs**: *On the Low-frequency Electromagnetic Waves in Quasi-Two-dimensional Metals*, Solid State Communications **146**, 8891 (2008).

11. D. H. Huang, **Godfrey Gumbs**, and M. Pepper: *Effects of inelastic capture, tunneling escape, and quantum confinement on surface acoustic wave-dragged photocurrents in quantum wells*, Journal of Applied Physics **103**, 083714 (2008).

12. Oleg Berman, Yurii Losovik, and **Godfrey Gumbs**: *Bose-Einstein condensation and Superfluidity of magnetoexcitons in Graphene*, Physical Review B **77**, 155433 (2008).

13. **Godfrey Gumbs**: *Semiconductor Photodetectors, Bio-material Sensors and Quantum Computers using High-Frequency Sound Waves*, AIP Conf. Proc. **991**, 57 (2008).

14. D. H. Huang, **Godfrey Gumbs**, Paul M. Alsing, and D. A. Cardimona: *Nonlocal mode mixing and surface-polariton-mediated enhancement of diffracted terahertz fields by a conductive grating*, Physical Review B **77**, 165404 (2008).

15. : D. H. Huang, **Godfrey Gumbs**, Paul M. Alsing, and David A. Cardimona: *Surface-polariton-enhanced Reflected THz-field*, PIERS Online Vol. **4**, No. 1, pp: 111-115 (2008).

16. Oleg L. Berman, **Godfrey Gumbs**, and Yurii E. Losovik: *Magnetoplasmons in Graphene Structures*, Proceedings of The 23rd PIERS 2008 in Hangzhou, CHINA 1158-1162 (2008).

17. Oleg L. Berman and **Godfrey Gumbs**: *Magnetoplasmons for an array of quantum dots in graphene*: Proceedings of The 24th PIERS 2008 in Cambridge, MA (2008).

18. D. H. Huang, **Godfrey Gumbs**, and M. Pepper: *Surface-Acoustic-Wave Based Quantum-Well Photodetectors*, Proc. SPIE **7095**, 70950I (2008).

19. Oleg L. Berman, **Godfrey Gumbs**, and Yurii E. Losovik: *Magnetoplasmons in layered graphene structures*, Physical Review B **78**, 085401 (2008).

20. Tibab McNeish, **Godfrey Gumbs**, and A. Balassis: *Plasmons for a two-Dimensional Array and a Bundle of nanotubes*, Physical Review B **77**, 235440 (2008).

21. S.J. Wright, M. D. Blumenthal, **Godfrey Gumbs**, A.L.T. Thorn, S.N. Holmes, T. J. B. M. Janssen, M. Pepper, D. Anderson, G.A.C. Jones, C.N. Nicoll: *Enhanced current quantization in high-frequency electron pumps in a perpendicular magnetic field*, Physical Review B **78**, 233311 (2008).

22. D. H. Huang, **Godfrey Gumbs**, and Shawn-Yu Lin: *Self-consistent theory for near-field distribution and spectrum with quantum wires and a conductive grating in terahertz regime*, . Journal of Applied Physics **105**, 093715 (2009) .

23. **Godfrey Gumbs**, D. H. Huang, and P. M. Echenique: *Comparing the Image Potential for Intercalated Graphene with a 2DEG with and without a periodic Grating*, Physical Review B **79** 035410 (2009).

24. Oleg L. Berman, **Godfrey Gumbs** and P. M. Echenique: *Quasiparticles for quantum dot array in graphene and the associated Magnetoplasmons*, Physical Review B **79**, 075418 (1-6) (2009).

25. D. H. Huang, S. K. Lyo, and **Godfrey Gumbs**: *Bloch oscillation, dynamical localization, and optical probing of electron gases in quantum-dot superlattices in high electric fields* , Physical Review B **79**, 155308 (1-19) (2009).

26. **Godfrey Gumbs** and D. H. Huang: *Magnetoquantum transport in a modulated 2D Electron Gas with Spin-orbit Interaction*, Physics Letters A **373**, 3506-3515 (2009).

27. Antonios Balassis, **Godfrey Gumbs**, and D. H. Huang: *Current-driven plasma instabilities for a bilayer two-dimensional electron system*, Proc. SPIE **7467**, 74670O (2009).

28. D. H. Huang and **Godfrey Gumbs**: *Coupled force-balance and scattering equations for nonlinear transport in quantum wires*, Physical Review B **80**, 033411 (1-4) (2009).

29. Natalya A. Zimbovskaya and **Godfrey Gumbs**: *Quantum oscillations in the high frequency magnetoacoustic response of a quasi-two-dimensional metal*, J. Phys.: Condens. Matter **21**, 415703-415709 (2009).

30. **Godfrey Gumbs**, D. H. Huang, Mark Blumenthal, S. J. Wright, M. Pepper, and Yonatan Abranyos: *Spin-Split Excitation Gap and Spin Entanglement of a Pair of Interacting Electrons in a Quantum Dot*, Semicond. Sci. and Technol. **24**, 115001 (2009).

31. A. Balassis and **Godfrey Gumbs**: *Enhanced Optical probe of current-driven coupled quantum wells*, Journal of Applied Physics **106**, 103102 (2009).

32. Oleg Berman, **Godfrey Gumbs**, and Patrick A. Folkes: *Collective Properties of Excitons in the Presence of a Two-Dimensional Electron Gas* , Solid State Communications **150**, 832-835 (2010).

33. O. Roslyak, A. Iurov, **Godfrey Gumbs**, and D. H. Huang: *Unimpeded Tunneling in Graphene Nanoribbons*, Journal of Physics: Condensed Matter **22**, 165301 (2010).

34. D. H. Huang and **Godfrey Gumbs**: *Comparison of inelastic and quasielastic scattering effects on nonlinear electron transport in quantum wires*, Journal of Applied Physics **107**, 103710 (2010).

35. O. Roslyak, **Godfrey Gumbs**, and D. H. Huang: *Tunable Band Structure Effects on Ballistic Transport in Graphene Nanoribbons*, Physics Letters A **374** 40614064 (2010).

36. Wen Xu, L. L. Li, H. M. Dong, **Godfrey Gumbs**, and Patrick Folkes: *Band hybridization and spin-splitting in InAs/AlSb/GaSb type II and broken-gap quantum wells*, Journal of Applied Physics **108**, 053709 (2010).

37. O. Roslyak, Shual Mukamel, and **Godfrey Gumbs**: *Signatures of carrier multiplication in polariton fluorescence spectra*, (Physics of Quantum Electronics) Journal of Modern Optics (2010).

38. L.-C. Tung, P. A. Folkes, **Godfrey Gumbs**, Wen Xu, and Y.-J. Wang: *IR modes in 2DEHGS Magneto-infrared modes in InAs-AlSb-GaSb coupled quantum wells*, Physical Review B **82**, 115305 (2010).

39. O. Roslyak, **Godfrey Gumbs**, and Shual Mukamel,: *Two-photon coincidence fluorescence spectra of cavity multi-polaritons; novel signatures of carrier multiplication*, Nano Letters **10**, 4253-4259 (2010).

40. O. Roslyak, **Godfrey Gumbs**, and D. H. Huang: *Klein Paradox and Tunable Band Structure Effects on Ballistic Transport in Graphene Nanoribbons*, Philosophical Transactions A of the Royal Society vol:**368**, 5431-5443 (2010).

41. **Godfrey Gumbs**, A. Balassis, and D. H. Huang: *Energy bands, conductance and thermoelectric power for ballistic electrons in a nanowire with spin-orbit interaction*, Journal of Applied Physics **108**, 093704 (2010).

42. Yonatan Abranyos, **Godfrey Gumbs**, and Paula Fekete: *Spin-dependent scattering by a potential barrier on a nanotube*, Journal of Physics: Condens. Matter **22**, 505304 (2010).

B. Book Publications

1. **Godfrey Gumbs** and D. H. Huang: *Interacting Properties of Low-Dimensional Systems*, (Wiley Press, NY) (2010), (*under contract for publication*) (see Fig.).

2. **Godfrey Gumbs**, D. H. Huang, and Oleksiy Roslyak: *"Electronic and Photonic Properties of Graphene Layers and Carbon Nanoribbons"*, Philosophical Transactions A of the Royal Society vol:**368**, # 1932 (2010) (see Fig.).

C. Conference Participation

1. **Godfrey Gumbs** and Antonios Balassis: *Absorption Coefficient for Cylindrical Nanotubes*, Bull. Am. Phys. Soc. **52**, (2007).

2. **Godfrey Gumbs**: *Magnetotransport in a Modulated 2DES* , Bull. Am. Phys. Soc. **52**, (2007).

3. **Godfrey Gumbs** and D. H. Huang: *Effect of Modulation on Coupled 2D-Surface Plasmons*, Bull. Am. Phys. Soc. **52**, (2007).

4. P. A. Folkes, **Godfrey Gumbs** and Wen Xu: *Measurement of the GaSb surface band bending potential from the magnetotransport characteristics of GaSb-InAs-AlSb quantum wells*, Bull. Am. Phys. Soc. **52**, (2007).

5. **Godfrey Gumbs**: *Semiconductor Photodetectors, Bio-material Sensors and Quantum Computers using High-Frequency Sound Waves*, National Society of Black Physicists, Boston, MA, 22-24 February (2007), (**Invited**).

6. W. Xu, P. A. Folkes, **Godfrey Gumbs**, Z. Zeng, and C. Zhang: *Electronic subband structure of InAs/GaSb based type II and broken- gap quantum well systems*, EP2DS (2007).

7. **Godfrey Gumbs** and Oleg Berman: *Magnetoplasmons in Graphene Multilayers*, Bull. Am. Phys. Soc. **53**, (2008).

8. Oleg Berman and **Godfrey Gumbs**: *BEC and Superfluidity of Magnetoexcitons in Graphene/*, Bull. Am. Phys. Soc. **53**, (2008).

9. D. H. Huang and **Godfrey Gumbs**: *Free-electron induced mode mixing and surface-polariton enhanced reflected THz-field* , Bull. Am. Phys. Soc. **53**, (2008).

10. **Godfrey Gumbs** and D. H. Huang: *Effects of capture, escape and confinement on SAW-dragged photocurrents in a single QW* , Bull. Am. Phys. Soc. **53**, (2008).

11. Hira Ghumman, Yu Gong, Cheng Wu, —bf Godfrey Gumbs, Yuhang Ren, Hassan Imrane, and Nian X. Sun, *Angular Dependence of Spin-wave resonance and relaxation in CoFeB/Cr superlattices*, National Society of Black Physicists Meeting, Baltimore, MD February (2008).

12. Li-Chun Tung, P. A. Folkes, —bf Godfrey Gumbs, Wen Xu, and Yong-Jie Wang: *Magneto-Infrared Study on 2-Dimensional Electrons and Holes in GaSb-AlSb-InAs Coupled Quantum Wells*, 29^{th} International Conference on the Physics of Semiconductors (ICPS), Rio de Janeiro, Brazil, July 27 - August 1 (2008).

13. Samuel Wright, Mark Blumenthal, **Godfrey Gumbs**. Adam Thorn, Michael Pepper, T. J. B. M. Jansen, Stuart Holmes, Dave Anderson, Geb Jones, Christine, Nicoll, and D. A. Ritchie: *Anomalous plateau formation and improved quantization in charge pumping under the application of a perpendicular magnetic eld* , Bull. Am. Phys. Soc. **54**, (2009).

14. Antonios Balassis and **Godfrey Gumbs**: *Grating-Enhanced Response for current-driven coupled quantum wells* , Bull. Am. Phys. Soc. **54**, (2009).

15. **Godfrey Gumbs**, D. H. Huang, and P. M. Echenique: *The Image Potential for Graphene with an electrostatic Grating* , Bull. Am. Phys. Soc. **54**, (2009).

16. S. J. Wright, **Godfrey Gumbs**, M. Pepper, M. D. Blumenthal, and D. H. Huang: *High-Frequency Electron Pumps used as an Entangler* , Bull. Am. Phys. Soc. **54**, (2009).

17. Oleg Berman, **Godfrey Gumbs**, and P. M. Echenique: *Quasiparticles for quantum dot array in graphene and the associated Magnetoplasmons* , Bull. Am. Phys. Soc. **54**, (2009).

18. Hira Ghumman and **Godfrey Gumbs**: *Tunneling Current for Graphene with Delta-Function Potential Scattering* , National Society of Black Physicists Meeting, Nashville, TN, February (2009).

19. Andrii Iurov, O. Roslyak, **Godfrey Gumbs**, and D. H. Huang: *Unimpeded Tunneling in Graphene Nanoribbons* , Bull. Am. Phys. Soc. **55**, (2010).

20. O. Roslyak, Andrii Iurov, **Godfrey Gumbs**, and D. H. Huang: *Tunable Band structure Effects on Ballistic Transport in Graphene Nanoribbons* , Bull. Am. Phys. Soc. **55**, (2010).

21. D. H. Huang and **Godfrey Gumbs**: *Nonlinear Electron Transport in Quantum Wires* , Bull. Am. Phys. Soc. **55**, (2010).

22. P. Folkes, L. C. Tung, **Godfrey Gumbs**, X. G. Wen, and Y. J. Wang: *Magneto-infrared modes in InAs-AlSb-GaSb coupled Coupled Quantum Wells*, Bull. Am. Phys. Soc. **55**, (2010).

23. **Godfrey Gumbs**, P. Folkes, and Oleg Berman: *Collective Properties of Excitons in the Presence of a two-dimensional electron gas*, Bull. Am. Phys. Soc. **55**, (2010).

24. Yonatan Abranyos and **Godfrey Gumbs**: *Spin Dependent Scattering in Nanotubes*, Bull. Am. Phys. Soc. **55**, (2010).

25. O. Roslyak, Shual Mukamel, and **Godfrey Gumbs**: *Signatures of carrier multiplication in polariton fluorescence spectra*, (Physics of Quantum Electronics) Snowbird, Utah, January 2-5 (2010).

26. **Godfrey Gumbs**: *conductance and thermoelectric power for ballistic electrons in a nanowire with spin-orbit interaction and Spin Current Tunneling on Nanotubes*, – (**Invited**) — Workshop on "Mesoscopic spin transport," 26 to 30 of April 2010, at the International Institute of Physics of Federal University of Rio Grande do Norte, Natal, Brasilia (**Invited**).

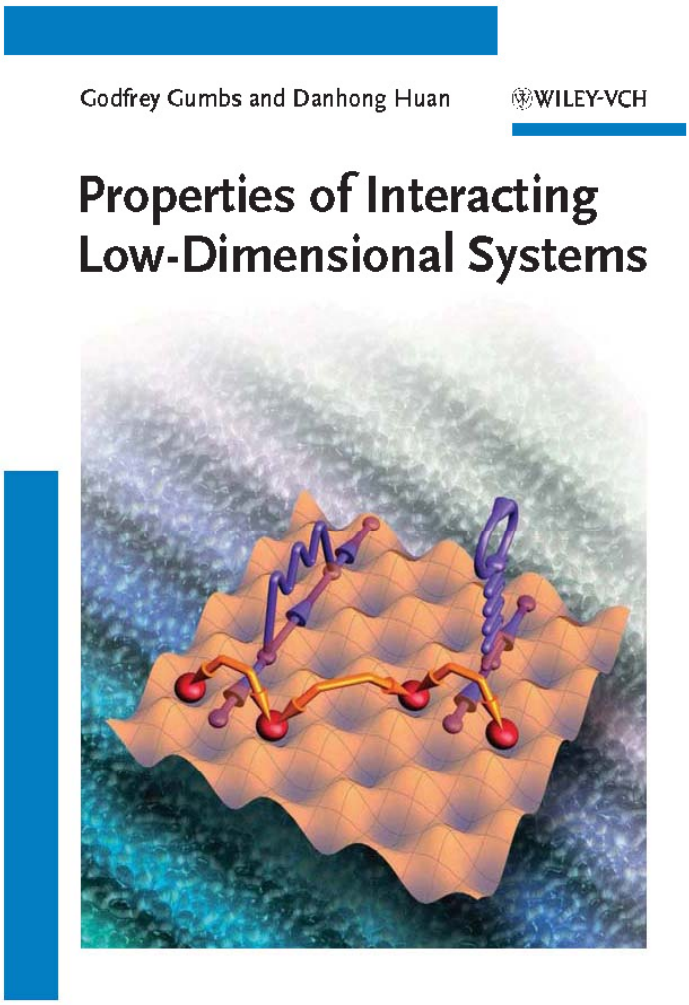

FIG. A-1: Copy of the book cover.

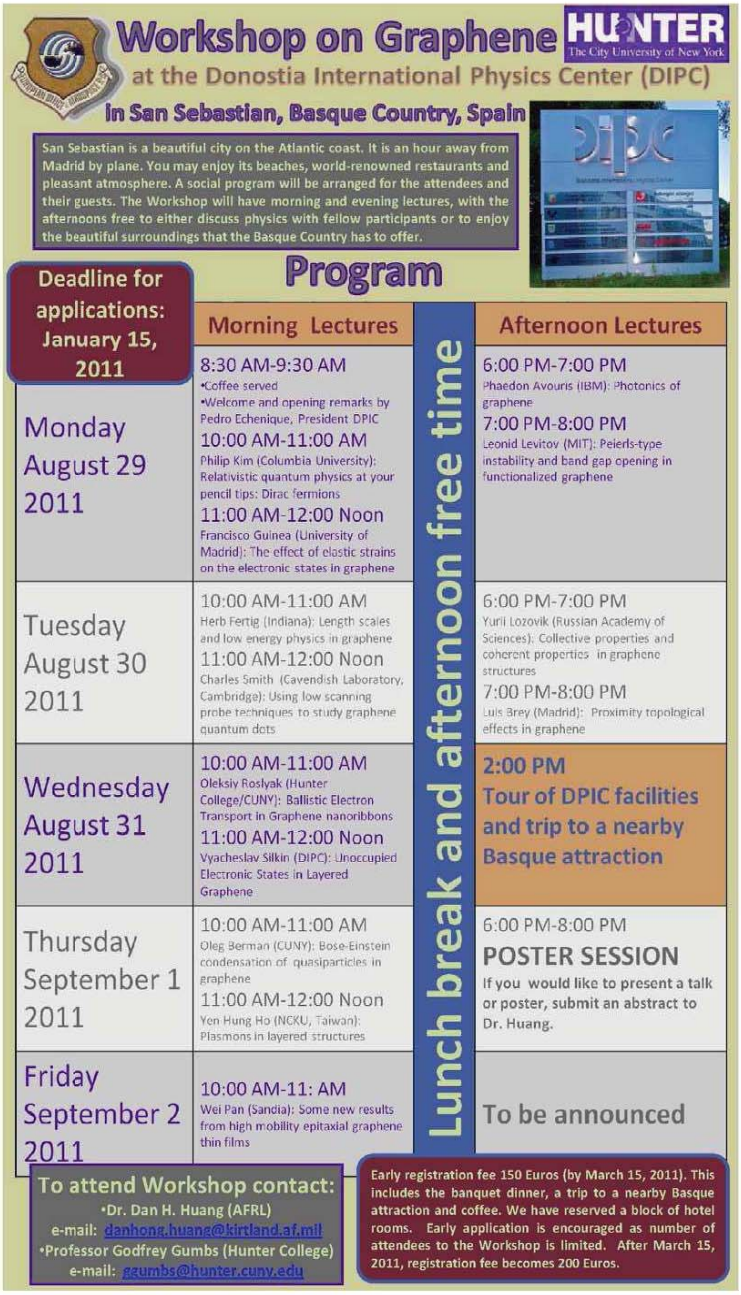

FIG. A-2: Copy of the graphene workshop flyer.

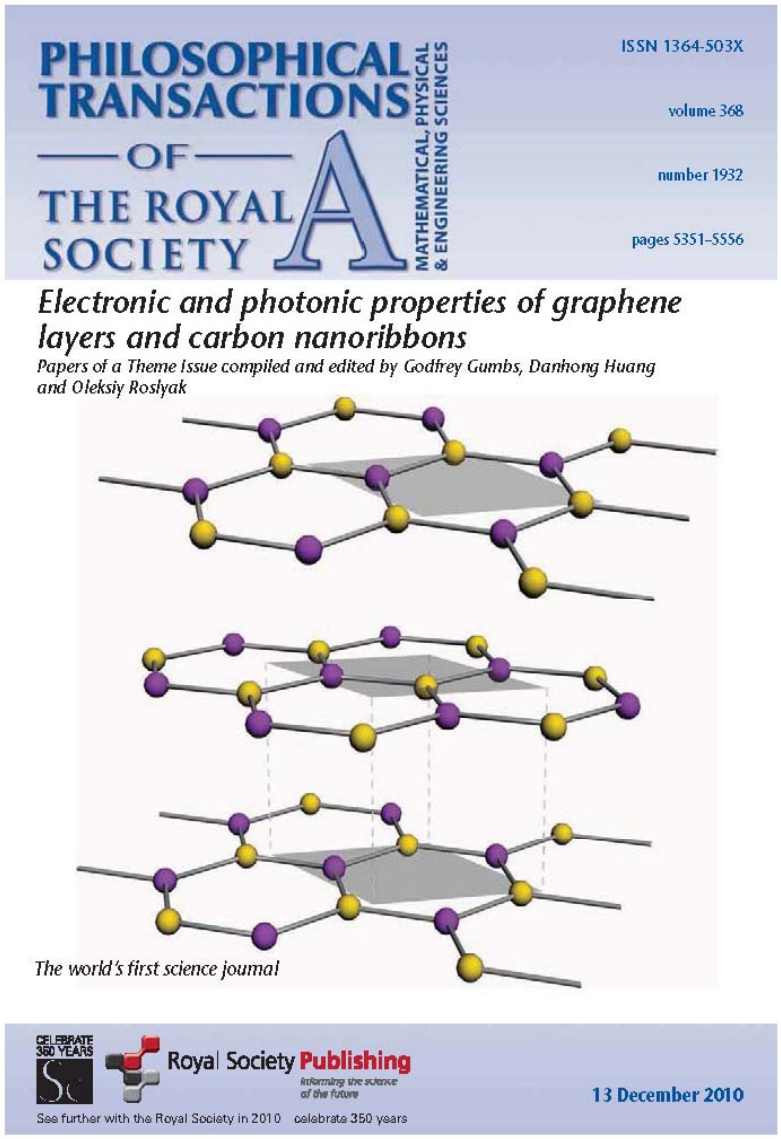

FIG. A-3: Copy of the journal special issue cover.

DISTRIBUTION LIST

DTIC/OCP
8725 John J. Kingman Rd, Suite 0944
Ft Belvoir, VA 22060-6218 1 cy

AFRL/RVIL
Kirtland AFB, NM 87117-5776 2 cys

Official Record Copy
AFRL/RVSS/Danhong Huang 1 cy

(This page intentionally left blank)